

The As-surface of an iron-based superconductor $\text{CaKFe}_4\text{As}_4$

Lu Cao^{1,2,§}, Yang Song^{1,2,§}, Ya-Bin Liu⁵, Qi Zheng^{1,2}, Guangyuan Han^{1,2}, Wenyao Liu^{1,2}, Meng Li^{1,2}, Hui Chen^{1,2}, Yuqing Xing^{1,2}, Guang-Han Cao⁵, Hong Ding^{1,3,4}, Xiao Lin^{1,2,3}, Shixuan Du^{1,2,3,4} (✉), Yu-Yang Zhang^{1,2,3}, Geng Li^{1,2,3,4} (✉), Ziqiang Wang⁶, and Hong-Jun Gao^{1,2,3,4} (✉)

¹ Institute of Physics, Chinese Academy of Sciences, Beijing 100190, China

² School of Physical Sciences, University of Chinese Academy of Sciences, Beijing 100049, China

³ CAS Center for Excellence in Topological Quantum Computation, University of Chinese Academy of Sciences, Beijing 100190, China

⁴ Songshan Lake Materials Laboratory, Dongguan 523808, China

⁵ Department of Physics, Zhejiang University, Hangzhou 310027, China

⁶ Department of Physics, Boston College, Chestnut Hill, Massachusetts 02467, USA

[§] Lu Cao and Yang Song contributed equally to this work.

© Tsinghua University Press and Springer-Verlag GmbH Germany, part of Springer Nature 2021

Received: 15 November 2020 / Revised: 16 December 2020 / Accepted: 4 January 2021

ABSTRACT

As a new type of iron-based superconductor, $\text{CaKFe}_4\text{As}_4$ has recently been demonstrated to be a promising platform for observing Majorana zero modes (MZMs). The surface of $\text{CaKFe}_4\text{As}_4$ plays an important role in realizing the MZM since it hosts superconducting topological surface states. However, due to the complicated crystal structure, the terminal surface of $\text{CaKFe}_4\text{As}_4$ has not been determined yet. Here, by using scanning tunneling microscopy/spectroscopy (STM/S), we find that there are two types of surface structure in $\text{CaKFe}_4\text{As}_4$. Bias-dependent atomic resolution images show an evolution from $\sqrt{2} \times \sqrt{2}$ superstructure with respect to the As lattice into 1×1 when the tip is brought close to the surface, revealing the sublattice of missing As atoms. Together with the first-principles calculations, we show that the surface As layer has a buckled structure. Our findings provide insight to future surface study of $\text{CaKFe}_4\text{As}_4$ as well as other iron-pnictide superconductors.

KEYWORDS

$\text{CaKFe}_4\text{As}_4$, scanning tunneling microscopy, atomic resolution, density functional theory

1 Introduction

As an important member of the iron-based superconductors, iron-pnictides have attracted tremendous attention in the past decade due to their unconventional pairing mechanisms and high transition temperatures (T_c) [1–8]. The quasi-2D structure of the As-Fe-As layers makes these materials facile to be cleaved and studied by surface-sensitive measurements such as scanning tunneling microscopy/spectroscopy (STM/S) [9] and angle-resolved photoemission spectroscopy (ARPES) [10]. Recently, based on a combined STM and ARPES study, $\text{CaKFe}_4\text{As}_4$ has been demonstrated as an emerging platform hosting Majorana zero modes [11]. The electronic structure of the cleaved surface has notable influence on the physical properties of $\text{CaKFe}_4\text{As}_4$ in the way of formation of topological surface states [12–15]. Therefore, determination of the atomic structure and electronic properties of the terminal surface is an important task for STM/S measurement [16, 17].

However, surface determination has never been an easy task in the iron-pnictide superconductors. In FeAs (111, stands for alkali atoms) systems, the cleavage happens at the central plane between two As-Fe-As layers, leaving two identical terminal surfaces which are nonpolar [9]. In AeFe_2As_2 (122, Ae stands for alkali-earth atoms) systems, however, the cleavage happens at the Ae-atom plane, giving rise to a controversial

terminal surface identification issue. For example, a typical $\sqrt{2} \times \sqrt{2}$ structure with respect to the As lattice has been detected by STM in different 122 systems [17–25]. Some reports claim that the $\sqrt{2} \times \sqrt{2}$ structure comes from the surface As layer with a tetragonal-to-orthorhombic transition [19, 21] or buckled structure [26]. However, the downward-buckled As atoms, or the “missing” atoms, have never been observed in previous STM studies. Others think that the alkali/alkali earth atoms (A/Ae) with a density of 0.5 atoms per unit cell on the surface [17, 18, 20, 23–25] contribute to the structure. Besides, surface reconstructions have also been observed on the surface of several 122 systems [17, 21, 27], making the surface determination even more complicated. In fact, in 122 systems, the structure of the terminal surface is a longstanding problem. Therefore, determination of the terminal surface in 122 systems is critical for further investigation of the electronic structure especially the unconventional superconductivity by STM/S. But so far, the atomic structures of the terminal surfaces of some 122 systems are still under debate [9, 17, 28], and observing the missing atoms is therefore crucial to solve this issue.

The $\text{AeAFe}_4\text{As}_4$ (1144) systems, with the A and Ae atoms alternately intercalated between the As-Fe-As layers, have similar lattice structure with the 122 systems [29, 30]. However, a different space group ($P4/mmm$) is expected due to the

inequivalent position of the A and Ae atoms [29]. This reduced lattice symmetry adds additional complexity to the surface identification issue in $\text{CaKFe}_4\text{As}_4$ (Fig. 1(a)). Here, we use STM/S to study the $\text{CaKFe}_4\text{As}_4$ terminal surfaces cleaved under 78 K. We identified an evolution of STM images from $\sqrt{2} \times \sqrt{2}$ superstructure with respect to the As lattice to 1×1 by varying the sample bias voltage. Quantum mechanical calculations based on density functional theory (DFT) find that there is a surface buckling in the As layer. This surface buckling breaks the symmetry of As layer and gives rise to the evolution of STM images under different bias voltages. Our work not only gives the unambiguous evidences of the As-terminated surface of $\text{CaKFe}_4\text{As}_4$ by observing the missing As sublattice, but also provides an instructive view to the surface determination issue of other iron-pnictide superconductors.

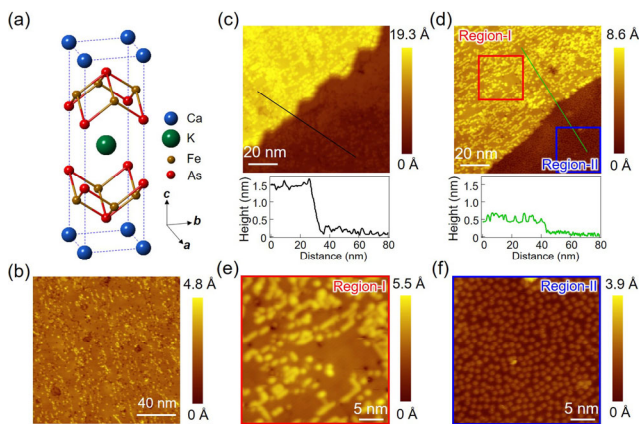


Figure 1 STM images of the $\text{CaKFe}_4\text{As}_4$ surface. (a) Unit cell of $\text{CaKFe}_4\text{As}_4$ crystalline lattice. (b) The large scale STM topography of the $\text{CaKFe}_4\text{As}_4$ cleaved at 78 K, showing randomly distributed bright clusters and dark pits. Setpoint: $V_s = -25$ mV, $I_t = -20$ pA. (c) The STM topography showing a step of the $\text{CaKFe}_4\text{As}_4$ surface of one unit cell. Setpoint: $V_s = -25$ mV, $I_t = -20$ pA. (d) The STM topography showing another kind of step of a half unit cell. The upper and lower terraces are assigned as region-I and region-II, respectively. Setpoint: $V_s = -25$ mV, $I_t = -20$ pA. (e) and (f) The zoom-in topography of region-I and region-II, respectively. Setpoint: $V_s = -25$ mV, $I_t = -20$ pA.

2 Results and discussion

Large scale STM image of $\text{CaKFe}_4\text{As}_4$ after cleavage at 78 K is shown in Fig. 1(b). The surface is mostly flat but with some imperfections such as randomly distributed bright clusters and dark pits, consistent with previous report [31]. The disordered feature has been observed in other 122 systems [19] and is attributed to scattered and clustered atoms whose lattice is destroyed by cleaving. Different from the 122 systems, cleavage may happen at either Ca or K planes, and we expect to see two types of terraces on the sample surface.

Indeed, two types of steps with different heights are observed. Figure 1(c) presents a step with a height of 1.31 ± 0.02 nm, agreeing with the lattice constant along c axis. As a result, the upper and the lower terraces are of the same type. The bright clusters distribute randomly on the terrace, leaving some small and clean spacings. Another type of step found on the surface is displayed in Fig. 1(d), with a typical height of 0.39 ± 0.02 nm. This step connects terraces of different types, which are assigned as region-I and region-II thereafter. We note that the step height in Fig. 1(d) is smaller than the half of the lattice constant (~ 0.64 nm). This inconsistency is probably due to the different contributions of the local density of states (LDOS) at the upper and lower terraces. We zoom in these two types of

terraces in Figs. 1(e) and 1(f). The clusters in region-I tend to assemble into irregular stripes, while the clusters in region-II disperse on the surface as isolated particles. In $\text{CaKFe}_4\text{As}_4$ lattice, the Fe-As bonding is strong and the Ca and K atoms intercalated between the As-Fe-As layers. The coupling between the Ca/K and As-Fe-As is weak compared with the Fe-As bond. When the cleavage happens at the Ca/FeAs layer or at K/FeAs layer, the Ca or K lattice is destroyed and the left-over Ca and K atoms on the surface aggregate to form irregular clusters. This naturally explains why two types of regions can be differentiated.

We now focus on the clean area of region-I. Figures 2(a)–2(f) show the atomic resolution images under different bias voltages. Under a sample bias of -40 mV, a square lattice can be resolved, as outlined by a blue square in Fig. 2(a). Line profile measurement (Fig. 2(g)) shows a periodicity of 5.6 ± 0.2 Å, suggesting a $\sqrt{2} \times \sqrt{2}$ structure with respect to the As lattice. Note that this $\sqrt{2} \times \sqrt{2}$ structure has been routinely observed on other 122 surfaces. Interestingly, reducing the bias to -2 mV (Fig. 2(f)) leads to the emergence of the missing sublattice of the As atoms. The newly emerged lattice has a periodicity of 3.9 ± 0.2 Å (Fig. 2(h)) and has a 45° rotation with respect to the lattice in Fig. 2(a), representing a 1×1 structure of the As lattice. The observation of STM image from $\sqrt{2} \times \sqrt{2}$ to 1×1 has been theoretically proposed to be critical evidence for surface determination in the 122 systems [26]. Upon cleavage, approximately half of Ca or K atoms are left on the surface which cannot form a 1×1 lattice. In fact, they tend to assemble into clusters due to the destroy of crystal lattice [19]. Therefore, the 1×1 structure can be safely assigned to the As layer. To the best of our knowledge, this is the first direct observation of the missing As atoms in the STM images evolution from $\sqrt{2} \times \sqrt{2}$ to 1×1 in 122 and 1144 systems.

In order to corroborate the above discussion, we carried out the first-principles calculations to investigate the bias-dependent STM images. It is found that, after the structural optimization, the superficial As atoms present a buckling of 0.12 Å (Fig. 3(a)) along c axis. The buckling results in two As sublattices, As_1 and As_2 , showing different projected density of states (PDOS) (Fig. 3(b)). Charge density was integrated with the energy range of (40, 100) meV (marked by cyan in Fig. 3(b)) and (-30 , 100) meV (marked by gray in Fig. 3(b)) to simulate the STM images under Tersoff-Hamann approximation [32]. We shifted the Fermi level to 100 meV because of two reasons: (1) the scattered Ca or K clusters on the As surface in the real system act as dopants which gives slight n-doping to the surface As

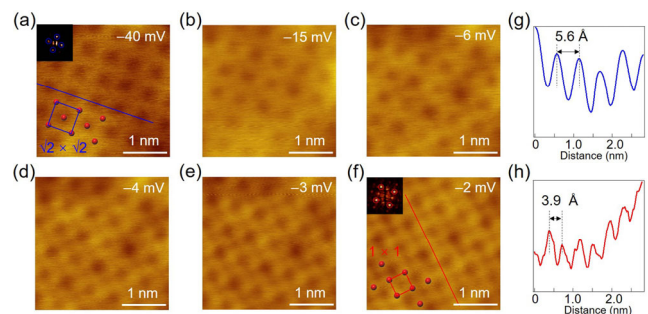


Figure 2 Atomic resolution STM images of the $\text{CaKFe}_4\text{As}_4$ surface with different bias. ((a)–(f)) STM topographies of the same region taken under different sample bias voltages. The blue and red squares outline the unit cell of two kinds of surface features, which show a $\sqrt{2} \times \sqrt{2}$ and a 1×1 structure with respect to the As lattice, respectively. Inset: the FFT of the real space lattices. The circles in FFT indicate the Bragg points. ((g) and (h)) Line profiles taken along the blue and red lines in (a) and (f), respectively.

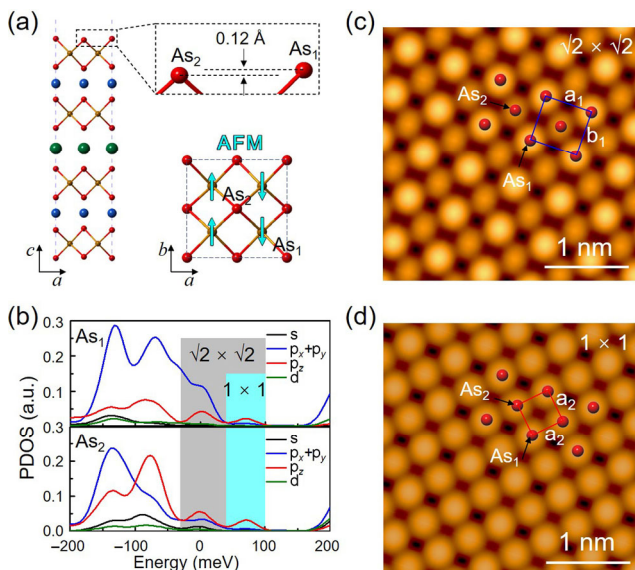


Figure 3 DFT calculated As-terminated surface. (a) The atomic structure of the slab model of the $\text{CaKFe}_4\text{As}_4$. The upper right panel shows the buckled As layer. The lower right panel shows the antiferromagnetic order of an As-Fe-As layer. The aqua arrows mark the magnetic moments of Fe atoms. (b) The PDOS of As_1 atom and As_2 atom. The integral energy ranges of the simulated $\sqrt{2} \times \sqrt{2}$ lattice and the 1×1 lattice are marked by gray and cyan, respectively. (c) Simulated STM image showing a $\sqrt{2} \times \sqrt{2}$ lattice. The lattice constant a_1 is 5.6 Å and b_1 is 5.5 Å. (d) Simulated STM image showing a 1×1 lattice. The lattice constant a_2 is 3.9 Å. From (c) to (d), the simulated results are consistent with the experimental observations.

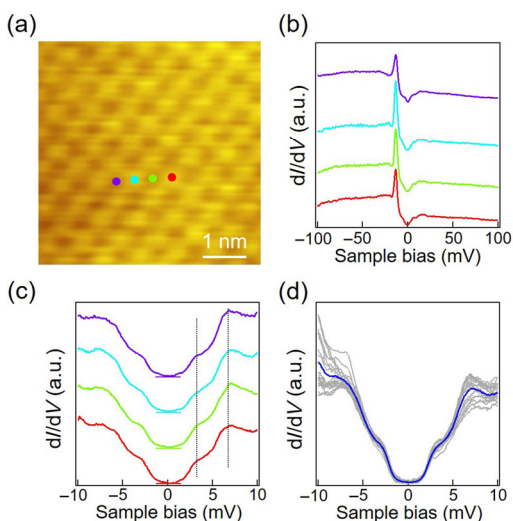


Figure 4 Local density of states of region-I in clean area. (a) The atomic resolution STM image. (b) Wide range dI/dV spectra taken at the locations marked in (a). The dI/dV spectra show uniform density of state in the clean areas, with a signature of Van Hove singularities at about -14 mV. Setpoint: $V_s = -50$ mV, $I_t = -200$ pA. (c) Zoom-in dI/dV spectra of (b). Superconducting gaps of ~ 7 meV and ~ 3 meV are observed (vertical dashed lines), corresponding to the nature of the multiple superconducting gaps of $\text{CaKFe}_4\text{As}_4$. Setpoint: $V_s = -5$ mV, $I_t = -200$ pA. The spectra in (b) and (c) are vertically offset for better comparison. (d) dI/dV spectra taken at different locations on the surface. The blue curve shows the averaged spectrum.

layer, and (2) the calculated PDOS shows lowest intensity around 100 meV, consistent with the lowest intensity of the dI/dV curve around zero-bias in Fig. 4(b). The $\sqrt{2} \times \sqrt{2}$ and the 1×1 lattice are observed under different bias voltages (Fig. 3(c) and 3(d)). The appearance of the $\sqrt{2} \times \sqrt{2}$ lattice is due to higher electronic states on As_1 than As_2 (Fig. 3(b)), which makes As_1 brighter than As_2 (Fig. 3(c)). Further analysis

of the PDOS images shows that the electronic states of $\sqrt{2} \times \sqrt{2}$ lattice are mainly contributed by in-plane p orbitals ($p_x + p_y$) of As_1 atom (blue line in the gray region of As_1), while the electronic states of 1×1 lattice are mainly contributed by out-of-plane p orbital (p_z) (red lines in the cyan region of As_1 and As_2). The STM image simulations are in good agreement with the experimental observations.

Apart from the different PDOS on As_1 and As_2 , another reason that the As_2 sublattice is difficult to resolve lies in its buckled nature. It is known that STM usually resolve only the topmost atoms in a buckled atomic layer since the spatial overlap of the wavefunctions between the tip and the downward-buckled atoms is small [33, 34]. For example, only half of the Si atoms in a buckled silicene layer on Ag(111) [33] and one-sixth of the Ge atoms in a buckled germanene layer on Pt(111) [34] can be visualized by STM. However, given the fact that the buckling of the As layer (0.12 Å) is much smaller than those in silicene or germanene, it is possible to resolve the lower As sublattice by bringing the tip in proximity to the sample surface. On the contrary, when the tip is lifted away from the surface under higher bias voltages, the overlap of the wavefunctions between the tip and the As_2 atoms will be smaller than that between the tip and the As_1 atoms, giving rise to larger contrast between As_1 and As_2 atoms in STM images than Fig. 3(c).

We tested different magnetic orders for the Fe layer and found the ground state is an antiferromagnetic (AFM) order. The magnetic moment directions of the Fe atoms in the upper Fe-As layer in the buckled structure are marked by cyan arrows in the lower right panel of Fig. 3(a). The magnetism along the longer side (a axis) is AFM and along the shorter side (b axis) is ferromagnetic (FM). We also calculated the Ca or K layers as terminal surfaces, but neither buckling nor lattice transition was found. Previous DFT study shows that the As-terminated surface of BaFe_2As_2 has a buckling of ~ 0.1 Å [26]. This result is consistent with our work where the DFT shows that, in $\text{CaKFe}_4\text{As}_4$, the As-terminated surface has a buckling of ~ 0.12 Å. This buckling leads to the evolution of STM topography from $\sqrt{2} \times \sqrt{2}$ to 1×1 under different bias voltages.

In spite of the buckled As surface, the dI/dV spectra taken along the clean area on region-I show uniform LDOS without any modulation (Fig. 4(b) and 4(c)). We note that the LDOS has lowest intensity at zero-bias accompanied with a strong particle-hole asymmetry around Fermi level as manifested by the significantly different LDOS intensity right below and above zero-bias [23, 25]. This particle-hole asymmetry is a reflection of the strongly correlated nature of $\text{CaKFe}_4\text{As}_4$ [23]. More than that, a signature of Van Hove singularities (VHS) can be seen in the dI/dV spectra in region-I, featured as sharp peaks below Fermi level at about -14 mV (Fig. 4(b)). Given the fact that the VHS is observed at -3.8 mV in KFe_2As_2 [23], $\text{CaKFe}_4\text{As}_4$ seems to be electron doped, which is reasonable if we assume that half K atoms are substituted by Ca. A higher doping level implies that region-I has excessive electrons which may be contributed by Ca. It is also worth noting that the dispersed clusters in region-II (Fig. 1(f)) resemble adsorbed K atoms on FeSe [35], $(\text{Li}_{0.8}\text{Fe}_{0.2}\text{OH})\text{FeSe}$ [36], and TaS_2 surface [37]. However, due to the lack of ability to identify different elements by STM, we cannot explicitly assign the adsorbates with Ca or K atoms. In the clean area, small range dI/dV spectra reveal the fully-opened superconducting (SC) gaps with a U-shape feature. SC gaps show two pairs of coherence peaks at ± 3 and ± 7 meV, suggesting the multiple SC gaps nature of $\text{CaKFe}_4\text{As}_4$ [11, 31, 38].

As a connate topological superconductor, the homogeneity

of the surface plays an important role in determining the occurrence of Majorana zero modes (MZMs). In the most widely studied connate topological superconductor Fe(Te,Se), doping of Te atoms gives rise to strong inhomogeneity of the surface at nanometer scale, leading to existence of topological trivial regions [14]. The inhomogeneity of the surface topology hampers future research in manipulation and braiding the vortices. On the other hand, CaKFe₄As₄ has much more homogeneous surface electronic state [11]. Our results demonstrate that despite the existence of slight buckling on the surface, the homogeneity of the surface electronic structure such as the VHS or SC gaps preserves at the nanometer scale. The uniform dI/dV spectra in Figs. 4(b) and 4(c) suggest that the surface buckling has little influence on the superconducting behavior as well as local Fermi level. For a statistical analysis, we have taken the superconducting spectra at different areas on the surface and summarize the result in Fig. 4(d). The small variation of the spectra feature corroborates again the homogeneous surface electronic states of CaKFe₄As₄, making it good platform in studying the MZMs. The determination of As-terminated surface is also important for further in-depth study of the MZMs in vortex and pairing mechanism of unconventional superconductivity in CaKFe₄As₄.

3 Conclusions

In conclusion, we have studied the surface termination of CaKFe₄As₄ by a combination of STM/S and DFT calculations. By resolving the missing As atoms on the surface, our results show that the cleaved surface of CaKFe₄As₄ is in fact the As lattice in Fe-As layer, with Ca and K clusters scattering on different terraces. DFT results confirmed the experimentally observed bias-dependent STM images from $\sqrt{2} \times \sqrt{2}$ to 1×1 are due to the buckling of the surface As layer. Our work not only uncovers the As layer termination of the CaKFe₄As₄ surface, but also provides a heuristic way to investigate the surface determination issue in other Fe-As superconductors.

4 Methods

4.1 STM/S

STM/S experiments were conducted in an ultrahigh vacuum (1×10^{-11} mbar) LT-STM system. Chemically etched tungsten tips were calibrated on Au(111) surface before use. The samples were cleaved at 78 K and transferred into the STM chamber immediately. STM images were acquired in the constant-current mode at 4.7 K. Differential conductance (dI/dV) spectra were acquired at 0.45 K by a standard lock-in amplifier at a frequency of 973.0 Hz under the modulation voltage $V_{\text{mod}} = 0.1$ mV.

4.2 DFT calculations

DFT calculations were implemented in the Vienna *ab-initio* simulation package (VASP) [39, 40] using projector-augmented wave (PAW) [41] method in conjunction with the Perdew–Burke–Ernzerhof (PBE) [42] functional. GGA+U was employed to optimize the geometric structures and U_{eff} was chosen as 1.2 eV for Fe by comparing with the lattice constant of experiment [43]. A slab containing fifteen atomic layers with a ($\sqrt{2} \times \sqrt{2}$) supercell was used to model the As-terminal surface. The in-plane size of the unit cell is $5.64 \text{ \AA} \times 5.48 \text{ \AA}$ (Fig. 3(a)). The vacuum layer is larger than 20 Å. The As-Fe-As slab of two surfaces were fully relaxed until the force on each atom was less than $0.01 \text{ eV} \cdot \text{Å}^{-1}$, while atoms in the middle layers were fixed. The plane-wave basis was set to an energy

cutoff of 400 eV. The Brillouin zone was sampled by a $(9 \times 9 \times 1)$ Gamma-centered k-mesh [44].

Acknowledgements

We thank Min Ouyang and Wu Zhou for helpful discussion. This work is supported by the National Key Research and Development Program of China (Nos. 2019YFA0308500 and 2018YFA0305800), the National Natural Science Foundation of China (Nos. 51922011, 51991340, and 61888102), the Strategic Priority Research Program of Chinese Academy of Sciences (No. XDB28000000). A portion of the research was performed in CAS Key Laboratory of Vacuum Physics. G. H. C. is supported by Funds for the Central Universities and the National Key Research and Development Program of China (Nos. 2019FZA3004, 2017YFA0303002, and 2016YFA0300202).

Reference

- [1] Kamihara, Y.; Watanabe, T.; Hirano, M.; Hosono, H. Iron-based layered superconductor La[O_{1-x}F_x]FeAs ($x = 0.05\text{--}0.12$) with $T_c = 26$ K. *J. Am. Chem. Soc.* **2008**, *130*, 3296–3297.
- [2] Paglione, J.; Greene, R. L. High-temperature superconductivity in iron-based materials. *Nat. Phys.* **2010**, *6*, 645–658.
- [3] Hirschfeld, P. J.; Korshunov, M. M.; Mazin, I. I. Gap symmetry and structure of Fe-based superconductors. *Rep. Prog. Phys.* **2011**, *74*, 124508.
- [4] Stewart, G. R. Superconductivity in iron compounds. *Rev. Mod. Phys.* **2011**, *83*, 1589–1652.
- [5] Wang, F.; Lee, D. H. The electron-pairing mechanism of iron-based superconductors. *Science* **2011**, *332*, 200–204.
- [6] Kordyuk, A. A. Iron-based superconductors: Magnetism, superconductivity, and electronic structure (Review Article). *Low Temp. Phys.* **2012**, *38*, 888–899.
- [7] Chen, X. H.; Dai, P. C.; Feng, D. L.; Xiang, T.; Zhang, F. C. Iron-based high transition temperature superconductors. *Natl. Sci. Rev.* **2014**, *1*, 371–395.
- [8] Si, Q. M.; Yu, R.; Abrahams, E. High-temperature superconductivity in iron pnictides and chalcogenides. *Nat. Rev. Mater.* **2016**, *1*, 16017.
- [9] Hoffman, J. E. Spectroscopic scanning tunneling microscopy insights into Fe-based superconductors. *Rep. Prog. Phys.* **2011**, *74*, 124513.
- [10] Richard, P.; Sato, T.; Nakayama, K.; Takahashi, T.; Ding, H. Fe-based superconductors: An angle-resolved photoemission spectroscopy perspective. *Rep. Prog. Phys.* **2011**, *74*, 124512.
- [11] Liu, W. Y.; Cao, L.; Zhu, S. Y.; Kong, L. Y.; Wang, G. W.; Papaj, M.; Zhang, P.; Liu, Y. B.; Chen, H.; Li, G. et al. A new Majorana platform in an Fe-As bilayer superconductor. *Nat. Commun.* **2020**, *11*, 5688.
- [12] Zhang, P.; Yaji, K.; Hashimoto, T.; Ota, Y.; Kondo, T.; Okazaki, K.; Wang, Z. J.; Wen, J. S.; Gu, G. D.; Ding, H. et al. Observation of topological superconductivity on the surface of an iron-based superconductor. *Science* **2018**, *360*, 182–186.
- [13] Wang, D. F.; Kong, L. Y.; Fan, P.; Chen, H.; Zhu, S. Y.; Liu, W. Y.; Cao, L.; Sun, Y. J.; Du, S. X.; Schneeloch, J. et al. Evidence for Majorana bound states in an iron-based superconductor. *Science* **2018**, *362*, 333–335.
- [14] Kong, L. Y.; Zhu, S. Y.; Papaj, M.; Chen, H.; Cao, L.; Isobe, H.; Xing, Y. Q.; Liu, W. Y.; Wang, D. F.; Fan, P. et al. Half-integer level shift of vortex bound states in an iron-based superconductor. *Nat. Phys.* **2019**, *15*, 1181–1187.
- [15] Zhu, S. Y.; Kong, L. Y.; Cao, L.; Chen, H.; Papaj, M.; Du, S. X.; Xing, Y. Q.; Liu, W. Y.; Wang, D. F.; Shen, C. M. et al. Nearly quantized conductance plateau of vortex zero mode in an iron-based superconductor. *Science* **2020**, *367*, 189–192.
- [16] Shan, L.; Wang, Y. L.; Shen, B.; Zeng, B.; Huang, Y.; Li, A.; Wang, D.; Yang, H.; Ren, C.; Wang, Q. H. et al. Observation of ordered vortices with Andreev bound states in Ba_{0.6}K_{0.4}Fe₂As₂. *Nat. Phys.* **2011**, *7*, 325–331.
- [17] Li, A.; Yin, J. X.; Wang, J. H.; Wu, Z.; Ma, J. H.; Sefat, A. S.; Sales, B. C.; Mandrus, D. G.; McGuire, M. A.; Jin, R. Y. et al. Surface

- terminations and layer-resolved tunneling spectroscopy of the 122 iron pnictide superconductors. *Phys. Rev. B* **2019**, *99*, 134520.
- [18] Masee, F.; de Jong, S.; Huang, Y.; Kaas, J.; van Heumen, E.; Goedkoop, J. B.; Golden, M. S. Cleavage surfaces of the $\text{BaFe}_{2-x}\text{Co}_x\text{As}_2$ and $\text{Fe}_3\text{Se}_{1-x}\text{Te}_x$ superconductors: A combined STM plus LEED study. *Phys. Rev. B* **2009**, *80*, 140507(R).
- [19] Nascimento, V. B.; Li, A.; Jayasundara, D. R.; Xuan, Y.; O'Neal, J.; Pan, S. H.; Chien, T. Y.; Hu, B.; He, X. B.; Li, G. R. et al. Surface geometric and electronic structures of $\text{BaFe}_2\text{As}_2(001)$. *Phys. Rev. Lett.* **2009**, *103*, 076104.
- [20] Zhang, H.; Dai, J.; Zhang, Y. J.; Qu, D. R.; Ji, H. W.; Wu, G.; Wang, X. F.; Chen, X. H.; Wang, B.; Zeng, C. G. et al. $\sqrt{2} \times \sqrt{2}$ structure and charge inhomogeneity at the surface of superconducting $\text{BaFe}_{2-x}\text{Co}_x\text{As}_2$ ($x = 0-0.32$). *Phys. Rev. B* **2010**, *81*, 104520.
- [21] Nishizaki, T.; Nakajima, Y.; Tamegai, T.; Kobayashi, N. Surface structure and superconductivity in $\text{Ba}(\text{Fe}_{0.93}\text{Co}_{0.07})_2\text{As}_2$ probed by scanning tunneling microscopy/spectroscopy. *J. Phys. Soc. Jpn.* **2011**, *80*, 014710.
- [22] Li, G. R.; He, X. B.; Zhang, J. D.; Jin, R. Y.; Sefat, A. S.; McGuire, M. A.; Mandrus, D. G.; Sales, B. C.; Plummer, E. W. Coupled structural and magnetic antiphase domain walls on BaFe_2As_2 . *Phys. Rev. B* **2012**, *86*, 060512(R).
- [23] Fang, D. L.; Shi, X.; Du, Z. Y.; Richard, P.; Yang, H.; Wu, X. X.; Zhang, P.; Qian, T.; Ding, X. X.; Wang, Z. Y. et al. Observation of a Van Hove singularity and implication for strong-coupling induced Cooper pairing in KFe_2As_2 . *Phys. Rev. B* **2015**, *92*, 144513.
- [24] Yang, X.; Du, Z. Y.; Lin, H.; Fang, D. L.; Yang, H.; Zhu, X. Y.; Wen, H. H. Vortex lattice and vortex bound states in CsFe_2As_2 investigated by scanning tunneling microscopy/spectroscopy. *Phys. Rev. B* **2018**, *98*, 024505.
- [25] Liu, X.; Tao, R.; Ren, M. Q.; Chen, W.; Yao, Q.; Wolf, T.; Yan, Y. J.; Zhang, T.; Feng, D. L. Evidence of nematic order and nodal superconducting gap along [110] direction in RbFe_2As_2 . *Nat. Commun.* **2019**, *10*, 1039.
- [26] Gao, M.; Ma, F. J.; Lu, Z. Y.; Xiang, T. Surface structures of ternary iron arsenides AFe_2As_2 ($A = \text{Ba, Sr, or Ca}$). *Phys. Rev. B* **2010**, *81*, 193409.
- [27] Li, G. R.; Liang, L. B.; Li, Q.; Pan, M. H.; Nascimento, V. B.; He, X. B.; Karki, A. B.; Meunier, V.; Jin, R. Y.; Zhang, J. D. et al. Role of antiferromagnetic ordering in the (1×2) surface reconstruction of $\text{Ca}(\text{Fe}_{1-x}\text{Co}_x)_2\text{As}_2$. *Phys. Rev. Lett.* **2014**, *112*, 077205.
- [28] Wilfert, S.; Schmitt, M.; Schmidt, H.; Mauerer, T.; Sessi, P.; Wang, H. D.; Mao, Q. H.; Fang, M. H.; Bode, M. Scanning tunneling microscopy and spectroscopy studies of the heavy-electron superconductor TlNi_2Se_2 . *Phys. Rev. B* **2018**, *97*, 014514.
- [29] Iyo, A.; Kawashima, K.; Kinjo, T.; Nishio, T.; Ishida, S.; Fujihisa, H.; Gotoh, Y.; Kihou, K.; Eisaki, H.; Yoshida, Y. New-structure-type Fe-based superconductors: CAFe_4As_4 ($A = \text{K, Rb, Cs}$) and $\text{SrAFe}_4\text{As}_4$ ($A = \text{Rb, Cs}$). *J. Am. Chem. Soc.* **2016**, *138*, 3410–3415.
- [30] Meier, W. R.; Kong, T.; Bud'ko, S. L.; Canfield, P. C. Optimization of the crystal growth of the superconductor $\text{CaKFe}_4\text{As}_4$ from solution in the $\text{FeAs}-\text{CaFe}_2\text{As}_2-\text{KFe}_2\text{As}_2$ system. *Phys. Rev. Mater.* **2017**, *1*, 013401.
- [31] Fente, A.; Meier, W. R.; Kong, T.; Kogan, V. G.; Bud'ko, S. L.; Canfield, P. C.; Guillamón, I.; Suderow, H. Influence of multiband sign-changing superconductivity on vortex cores and vortex pinning in stoichiometric high- T_c $\text{CaKFe}_4\text{As}_4$. *Phys. Rev. B* **2018**, *97*, 134501.
- [32] Tersoff, J.; Hamann, D. R. Theory and application for the scanning tunneling microscope. *Phys. Rev. Lett.* **1983**, *50*, 1998–2001.
- [33] Vogt, P.; De Padova, P.; Quaresima, C.; Avila, J.; Frantzeskakis, E.; Asensio, M. C.; Resta, A.; Ealet, B.; Le Lay, G. Silicene: Compelling experimental evidence for graphenelike two-dimensional silicon. *Phys. Rev. Lett.* **2012**, *108*, 155501.
- [34] Li, L. F.; Lu, S. Z.; Pan, J. B.; Qin, Z. H.; Wang, Y. Q.; Wang, Y. L.; Cao, G. Y.; Du, S. X.; Gao, H. J. Buckled germanene formation on $\text{Pt}(111)$. *Adv. Mater.* **2014**, *26*, 4820–4824.
- [35] Song, C. L.; Zhang, H. M.; Zhong, Y.; Hu, X. P.; Ji, S. H.; Wang, L. L.; He, K.; Ma, X. C.; Xue, Q. K. Observation of double-dome superconductivity in potassium-doped FeSe thin films. *Phys. Rev. Lett.* **2016**, *116*, 157001.
- [36] Ren, M. Q.; Yan, Y. J.; Niu, X. H.; Tao, R.; Hu, D.; Peng, R.; Xie, B. P.; Zhao, J.; Zhang, T.; Feng, D. L. Superconductivity across Lifshitz transition and anomalous insulating state in surface K-dosed $(\text{Li}_{0.8}\text{Fe}_{0.2}\text{OH})\text{FeSe}$. *Sci. Adv.* **2017**, *3*, e1603238.
- [37] Zhu, X. Y.; Wang, S.; Jia, Z. Y.; Zhu, L.; Li, Q. Y.; Zhao, W. M.; Xue, C. L.; Xu, Y. J.; Ma, Z.; Wen, J. S. et al. Realization of a metallic state in $1T-\text{TaS}_2$ with persisting long-range order of a charge density wave. *Phys. Rev. Lett.* **2019**, *123*, 206405.
- [38] Mou, D. X.; Kong, T.; Meier, W. R.; Lochner, F.; Wang, L. L.; Lin, Q. S.; Wu, Y.; Bud'ko, S. L.; Eremin, I.; Johnson, D. D. et al. Enhancement of the superconducting gap by nesting in $\text{CaKFe}_4\text{As}_4$: A new high temperature superconductor. *Phys. Rev. Lett.* **2016**, *117*, 277001.
- [39] Kresse, G.; Hafner, J. *Ab initio* molecular dynamics for liquid metals. *Phys. Rev. B* **1993**, *47*, 558–561.
- [40] Kresse, G.; Furthmüller, J. Efficiency of *ab-initio* total energy calculations for metals and semiconductors using a plane-wave basis set. *Comp. Mater. Sci.* **1996**, *6*, 15–50.
- [41] Blöchl, P. E. Projector augmented-wave method. *Phys. Rev. B* **1994**, *50*, 17953–17979.
- [42] Perdew, J. P.; Burke, K.; Ernzerhof, M. Generalized gradient approximation made simple. *Phys. Rev. Lett.* **1996**, *77*, 3865–3868.
- [43] Anisimov, V. I.; Zaanen, J.; Andersen, O. K. Band theory and Mott insulators: Hubbard U instead of stoner I . *Phys. Rev. B* **1991**, *44*, 943–954.
- [44] Monkhorst, H. J.; Pack, J. D. Special points for Brillouin-zone integrations. *Phys. Rev. B* **1976**, *13*, 5188–5192.